

On-chip transverse-mode entangled photon source

Lan-Tian Feng^{*,1,2} Ming Zhang^{*,3} Xiao Xiong^{1,2} Yang Chen^{1,2} Hao Wu³ Ming Li³ Guo-Ping Guo^{1,2} Guang-Can Guo^{1,2} Dao-Xin Dai^{†,3} and Xi-Feng Ren^{‡1,2}

¹Key Laboratory of Quantum Information, University of Science and Technology of China, CAS, Hefei, 230026, People's Republic of China.

²Synergetic Innovation Center of Quantum Information & Quantum Physics,
University of Science and Technology of China, Hefei, Anhui 230026, China.

³State Key Laboratory for Modern Optical Instrumentation, Centre for Optical and Electromagnetic Research,
Zhejiang Provincial Key Laboratory for Sensing Technologies,
Zhejiang University, Zijingang Campus, Hangzhou 310058, China.

An on-chip photonic quantum source, especially an on-chip entangled photon source, is an essential resource for quantum information applications. Here, we report an on-chip transverse-mode entangled photon source, which is realized using spontaneous four-wave mixing processes in a multimode silicon waveguide. Transverse-mode entangled photon pairs are generated and experimentally verified with a bandwidth of $\sim 2\text{ THz}$; a maximally transverse-mode entangled Bell state can also be produced with a fidelity of 0.92 ± 0.01 . The demonstrated on-chip entangled photon source provides one of the most important key elements for developing quantum photonics using transverse-mode freedom, which can be used to encode quantum information within a high-dimensional Hilbert space. And the transverse-mode entanglement can be converted coherently to path and polarization entanglement on-chip. This paves the way to realize highly complex quantum photonic circuits with multiple degrees of freedom and plays an important role in the high-dimensional quantum information processing.

INTRODUCTION

Quantum source is not only critical to advancing our understanding of quantum mechanics, but also play a key role in generating many applications in quantum technologies [1]. Compared with free-space ones, integrated quantum photonic sources have attracted much attention owing to their compactness, scalability, and stability [2]. For example, path or polarization entangled sources were demonstrated by using the nonlinear processes in a singlemode waveguide or in a micro-ring cavity [3–7]. More recently, a new quantum information encoder based on transverse-modes in a multimode optical waveguide was introduced to quantum photonics [8, 9]. Such a development is very attractive because orthogonal transverse-modes in a multimode waveguide constitute a high-dimensional Hilbert space, which is useful for parallel encoding and enables one to encode more information per photon for next-generation classical optical communications [10–13]. The high-dimensional encoding space can also be used to achieve special entangled states, such as high-dimensional entangled states [6] and hyper-entangled states [14], which results in more efficient quantum logic gates and noise-resilient communications [15, 16]. Besides, transverse-mode entanglement can be converted coherently to path and polarization entanglement [8], which showed the possibility to control multiple degrees of freedom of photons simultaneously. However, an on-chip transverse-mode entangled photon source has not yet been realized.

Here, we propose and realize for the first time an on-chip transverse-mode entangled photon source by utilizing spontaneous four-wave mixing (SFWM) processes in a multimode silicon nanophotonic waveguide. Transverse-mode entangled photon pairs are generated and experimentally verified with a bandwidth of $\sim 2\text{ THz}$. By adjusting the energy ratio and phase difference between different transverse-mode terms of the pump light, a maximally transverse-mode entangled Bell state is produced with a fidelity of 0.92 ± 0.01 . Our protocol can definitely be generalized to cases of high-dimensional entangled photon sources with more transverse-modes, thus shows potential for realizing complex quantum information processes with high dimensionality and multiple degrees of freedom.

* These authors contributed equally to this work.

† dxddai@zju.edu.cn

‡ renxf@ustc.edu.cn

RESULTS

Entangled photon source chip

As shown in Fig. 1a, the device includes three parts: a mode modulator, a multimode waveguide and an output state analyser, as illustrated in Fig. 1a. The mode modulator is used to modulate the pump power ratio for different transverse-modes, and the output state analyser is used to export the state for measurement. The multimode waveguide is 3 mm long, with a cross-section of $\sim 760 \times 220 \text{ nm}^2$, so that it can support two transverse-electric (TE) modes, i.e., TE_0 and TE_1 . The pump light is coupled to the device through a grating coupler and then divided into two parts through a directional coupler, with one part being converted to the transverse-mode TE_0 and the other to the transverse-mode TE_1 through a mode multiplexer [10]. After nonlinear interactions in the multimode waveguide, a mode demultiplexer is used to separate the generated photons into different paths, which are then coupled out using two identical grating couplers for further measurement.

The SFWM processes in our device can be divided into three types (see Supplementary Text). For Type I, the four photons involved are in the same transverse-mode. For Type II, the two pump photons are in the same transverse mode, while the signal and idler photons are in the other transverse mode. For Type III, the two pump photons are in different transverse modes (i.e., one in TE_0 and the other in TE_1), and the signal and idler photons are also in different transverse modes. The SFWM process of Type I is intramodal, while the SFWM processes of Type II and Type III are intermodal. Here, the phase mismatching for the Type II process is so large that it hardly occurs. Therefore, we focus on Type I and Type III processes, where the signal and idler photon pairs have four combinations of transverse modes, i.e., $|TE_0TE_0\rangle$, $|TE_1TE_1\rangle$, $|TE_0TE_1\rangle$ and $|TE_1TE_0\rangle$ (Fig. 1b). We calculated the first-order dispersions β_1 and second-order dispersions β_2 of the multimode waveguide for the TE_0 and TE_1 modes, respectively (Fig. 1c). The normalized net magnification factor \hat{S} of the generated photon pairs for those four transverse-mode combinations is shown in Fig. 1d. The signal and idler photons are time correlated, and their frequencies are equally separated from the central pump frequency.

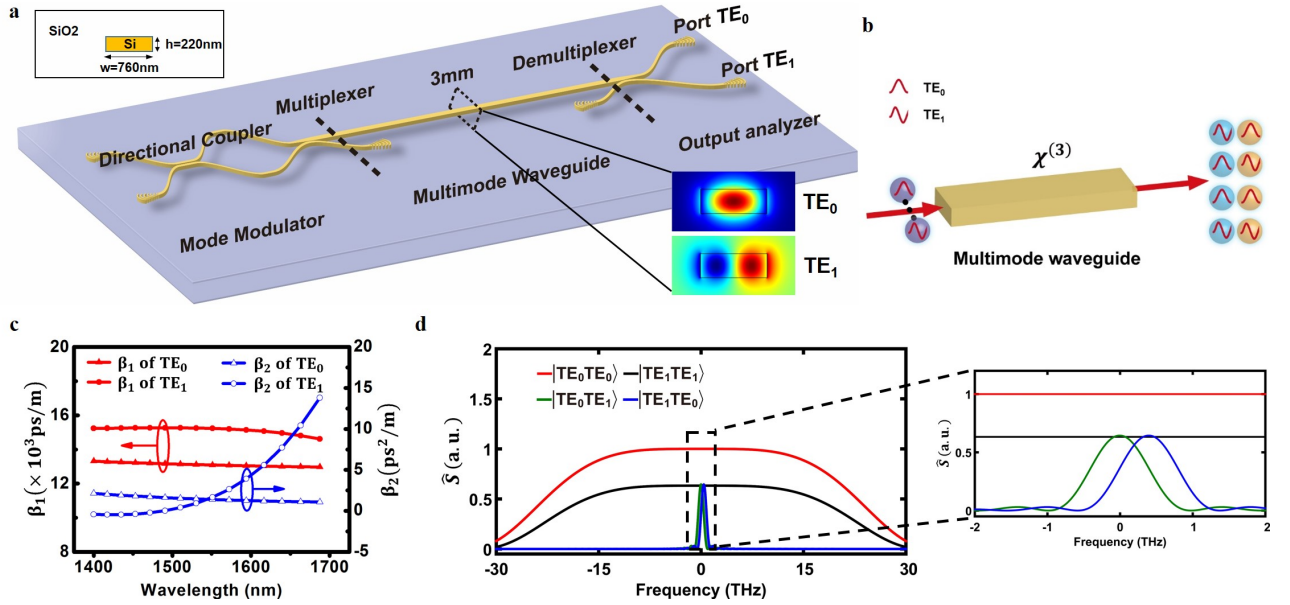


FIG. 1: **Schematic of the sample, concept of photon-pair generation and theoretical calculations.** **a**, Schematic of the sample, including a mode modulator, a multimode waveguide, and an output analyser. Insets: cross-section of the multimode waveguide (upper left) and the E_x components of the transverse-modes TE_0 and TE_1 (lower right). **b**, concept of photon-pair generation in a multimode waveguide. Pump photons can be in the same or different transverse modes, and the generated idler and signal photons will be in multiple transverse-mode combinations. The SFWM processes in the multimode waveguide will generate correlated photon pairs in four kinds of transverse-mode combinations, i.e., $|TE_0TE_0\rangle$, $|TE_1TE_1\rangle$, $|TE_0TE_1\rangle$ and $|TE_1TE_0\rangle$. **c**, The calculated value for the first-order and second-order dispersions of the multimode waveguide for TE_0 and TE_1 modes. **d**, Calculated normalized net magnification factor for four kinds of transverse-mode combinations of the generated photon pairs. The curves for $|TE_0TE_1\rangle$ (green) and $|TE_1TE_0\rangle$ (blue) coincide, so we shifted the blue curve by 0.4 THz for a better view. Inset: zoom-in view.

Transverse-mode entanglement verification

To ascertain the generated quantum states, we measured the photon pair coincidence for different combinations of the frequency and transverse-mode. As shown in Fig. 2a, an amplified continuous-wave (CW) laser (central wavelength 1550.11 nm) was coupled to the device via a grating coupler by a single-mode fibre array after passing through two cascaded 100 GHz bandwidth pre-filters. The SFWM processes, which produce correlated photon pairs, mainly occurred in the multimode waveguide. At the output end, the pump light was blocked by two cascaded off-chip 200 GHz bandwidth post-filters. Two 40-channel wavelength-division-multiplexers (WDMs) were used to separate the signal and idler photons. Each channel has a 100 GHz bandwidth, such that we can select any frequency- and transverse-mode combinations for photon pairs with a frequency detuning ~ 2 THz from the central pump frequency (Supplementary Table 3). The generated photon pairs were finally detected by two superconducting nanowire single-photon detectors (SCONTEL, dark count rate 100 Hz, detection efficiency 85%).

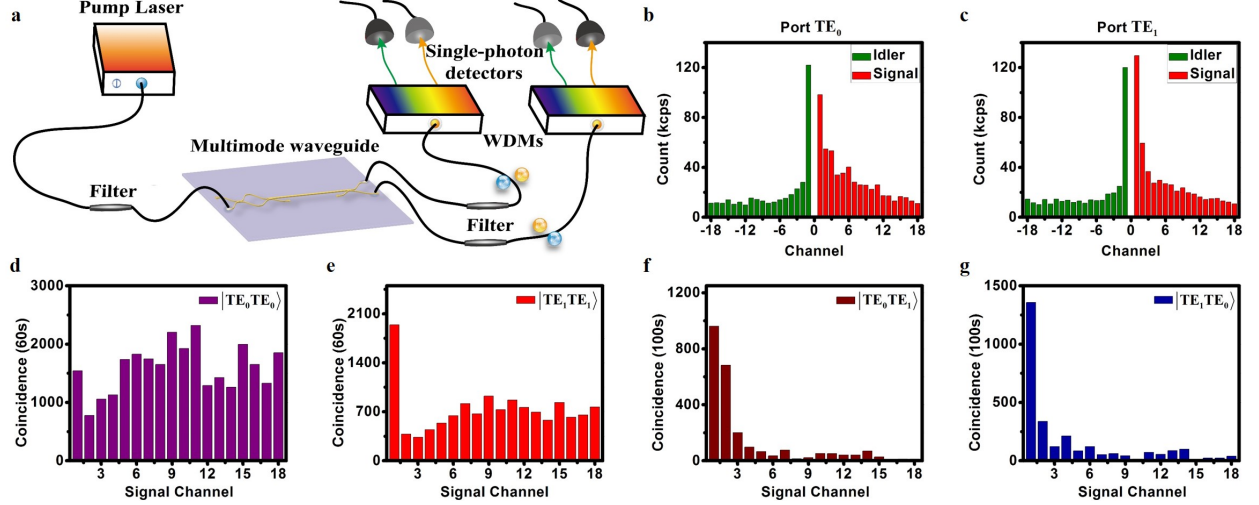


FIG. 2: **Sketch map for the experimental setup and measurement results.** **a**, An amplified CW laser is coupled to the device via a fibre array, and two WDMs are used to separate the idler, signal and pump photons into different frequencies. **b** and **c**, The continuous emission spectra for the signal and idler photons from ports TE_0 and TE_1 , respectively. The spectra are filtered by a 40-channel WDMs system, with the frequencies of the correlated photon pairs equally separated from the central pump frequency. **d-g**, Coincidence measurement of the photon pairs in different transverse-mode combinations.

We measured single photon counts in different frequency channels, as shown in Fig. 2b,c. The differences in single photon count arise from the different gains for the SFWM processes and the uneven Raman scattering and losses for different WDMs channels. To further characterize the photon source in the multimode waveguide, we also measured the coincidence counts for the processes of Type I (Fig. 2d,e) and Type III (Fig. 2f,g) processes. All coincidences are the raw data without subtracting the background and accident counts. As seen, accompanied by oscillation, the coincidences for the Type III process decrease as the frequency detuning increases, which agrees well with the theoretical calculations (Fig. 1d). Note that the photon pairs were collected with a longer integral time for the Type III process due to its lower generation rates.

Coincidence-to-accidental ratio (CAR) and source brightness are two key parameters for characterizing the photon pair source. We measured CARs for correlated photon pairs in different transverse-mode combinations (Supplementary Fig. 1). Intramodal (Type I) photon pairs show high CARs (generally higher than 200 for $|TE_0TE_0\rangle$ and 100 for $|TE_1TE_1\rangle$), while the CARs for the intermodal photon pairs (Type III) are not high (lower than 10 in most cases) because of the large phase mismatching. It is possible to obtain higher CARs by broadening the frequency spectra with a wider multimode waveguide, benefiting from a smaller difference in the first-order dispersion between signal and idler photons.

In a wider multimode waveguide, the lower energy density enables a better tolerance to nonlinear noise; thus, one can simultaneously improve the brightness and the CARs by simply increasing the input pump power. In the experiment, we measured the photon pair $|TE_0TE_0\rangle$ ($|TE_1TE_1\rangle$) with a calculated generation rate changing from 19 kHz (5.5 kHz) to 530 kHz (180 kHz). It can be seen that the CARs do not suffer an obvious reduction even at the highest generation rates (Supplementary Fig. 2). These results show that the present device provides a flexible platform for quantum information processing.

The previous measurements revealed frequency and transverse-mode correlations between the generated photon pairs. We then went further to demonstrate the generation of quantum entanglement, which lies at the heart of quantum information

studies [17]. As described above, the quantum state in the multimode waveguide is given as

$$|\Phi\rangle = \frac{1}{\sqrt{1 + \eta_1^2 + \eta_2^2 + \eta_3^2}} (|TE_1TE_1\rangle + \eta_1 e^{i\delta_1} |TE_1TE_0\rangle + \eta_2 e^{i\delta_2} |TE_0TE_1\rangle + \eta_3 e^{i\delta_3} |TE_0TE_0\rangle), \quad (1)$$

where η_1, η_2 and η_3 are relative proportions of different components; δ_1, δ_2 and δ_3 are the phase differences, which come from the mode dispersions in the multimode waveguide. By using a two-dimensional (2D) grating coupler [18, 19], the transverse-mode entangled state was coherently converted into the polarization entangled state, which is expressed as $|\Phi\rangle = \frac{1}{\sqrt{1 + \eta_1^2 + \eta_2^2 + \eta_3^2}} (|HH\rangle + \eta_1 e^{i\delta_1} |HV\rangle + \eta_2 e^{i\delta_2} |VH\rangle + \eta_3 e^{i\delta_3} |VV\rangle)$.

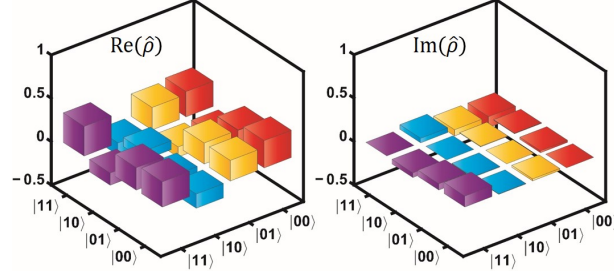


FIG. 3: **Quantum state characterization of photon pairs in the frequency channels ± 2 by means of tomography.** A quantum state can be fully described by its density matrix $\hat{\rho}$. The real (Re) and imaginary (Im) parts of the density matrix of the quantum state in the frequency channels ± 2 were provided. Here, we use 1 to represent the transverse mode TE_1 and 0 to represent the transverse mode TE_0 .

According to Fig. 1d and Fig. 2d-g, when the frequencies of the signal and idler photons are close to the pump frequency, all four transverse-mode combinations are generated. As an example, we performed a quantum state tomography measurement [20] for the photon pairs in the frequency channels ± 2 , and the results are shown in Fig. 3. The normalized state was estimated as $|\Phi\rangle = 0.60 |TE_1TE_1\rangle + 0.29 e^{-2.8i} |TE_1TE_1\rangle + 0.48 e^{0.29i} |TE_0TE_1\rangle + 0.57 e^{0.40i} |TE_0TE_0\rangle$, with a fidelity of 0.92 ± 0.02 . The high fidelity unambiguously shows that both intramodal and intermodal photon pairs are generated and that they constitute a complex but pure quantum state.

Transverse-mode entangled Bell state generation

More interestingly, in some channels, intermodal photon pairs are negligible such that the entangled state

$$|\Phi\rangle = \frac{1}{\sqrt{1 + \eta_3^2}} (|TE_1TE_1\rangle + \eta_3 e^{i\delta_3} |TE_0TE_0\rangle) \quad (2)$$

can be acquired. Furthermore, by adjusting the energy ratio and the phase difference between the TE_0 and TE_1 terms for the pump light, one can achieve a maximally transverse-mode entangled state as follows:

$$|\Phi\rangle = \frac{1}{\sqrt{2}} (|TE_1TE_1\rangle + |TE_0TE_0\rangle). \quad (3)$$

We took the frequency channels ± 8 to test the quality of the entanglement. First, the two-photon polarization interference fringes were measured, as given in Fig. 4a. The raw visibilities in the 0° (solid black line) and 45° (solid red line) bases were $95.0 \pm 1.8\%$ and $98.6 \pm 1.6\%$, which are both greater than $\frac{1}{\sqrt{2}} \approx 70.7\%$, confirming entanglement through violation of the Clauser-Horne-Shimony-Holt (CHSH) inequality.

Then, quantum state tomography was performed to measure the state density matrix $\hat{\rho}$. The ideal density matrix of the maximally entangled state in Eq. (3) and the measured density matrix of the output state from frequency channels ± 8 are shown in Fig. 4b and c, respectively. We used the maximum-likelihood-estimation method [20] to construct the density matrix using the experimental results. The fidelity is defined as $F = \text{Tr}(\hat{\rho}_{exp} \hat{\rho}_{th})$, where Tr is the trace, $\hat{\rho}_{exp}$ is the measured density matrix, and $\hat{\rho}_{th}$ is the ideal density matrix. We obtained a fidelity of 0.92 ± 0.01 , confirming that the generated quantum state is of high quality and very close to the ideal maximally entangled state. The errors in fidelity were obtained by 100 times Monto Carlo calculation, with the experimental data subject to Gaussian statistics. The deviation of the fidelity from unity was mainly due to the unbalanced power splitting ratio for the different transverse modes. Through use of a cascading on-chip Mach-Zehnder interferometer with thermal tuning to regulate the energy distribution and phase of different transverse modes, any level of biphoton entanglement can be achieved.

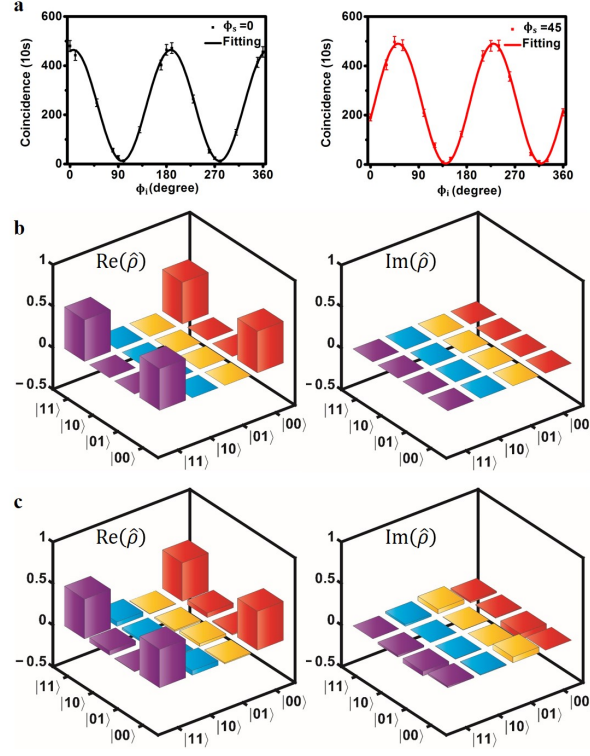


FIG. 4: **Quantum state characterization of photon pairs in the frequency channels ± 8 through interference and state tomography.** **a**, Coincidences in 10 s intervals as a function of the idler polarizer angle when the signal polarizer is held at 0° (solid black line) and 45° (solid red line), respectively. **b**, The real (Re) and imaginary (Im) parts for the density matrix of the ideal maximally entangled Bell state. **c**, The measured density matrix of the quantum state agrees well with the ideal case. Here, we use 1 to represent the transverse mode TE_1 and 0 to represent the transverse mode TE_0 .

DISCUSSION

Although only two transverse-modes were used in the experiment, our protocol can definitely be generalized to cases with more transverse-modes. By introducing multi-channel mode multiplexers to modulate the transverse-modes of the pump light, a high-dimensional transverse-mode entangled state can be directly generated in a multimode waveguide. The transverse-mode entangled state can be coherently converted into path and polarization entanglement, which provides convenience for large-scale quantum photonic integrated circuits (QPICs)[21–29] and hyper-entanglement generation [14]. Due to the non-uniform intermodal nonlinear process, photon pairs in different frequency channels are in different quantum states; thus, we can choose the quantum state as desired by selecting frequency channels, which is unimaginable for a single-mode waveguide. This frequency-multiplexed transverse-mode entangled photon pair source in a multimode waveguide offers high selectivity and flexibility for realizing quantum applications.

In addition, photons in different transverse-modes can participate in the same nonlinear interaction simultaneously, which leads to much richer nonlinear phenomena compared to a single-mode waveguide [30, 31]. Several works have been done to investigate the nonlinear process with multiple modes, such as wavelength conversion in a multimode waveguide [32–34], and photon pair generation in a few mode fiber [35], as well as a periodically poled KTiOPO4 multimode waveguide [36], which showed the advantages over a single-mode waveguide. For example, the intermodal SFWM process, where both the first-order and second-order dispersions can be engineered for phase matching, can be used to realise conversion between widely separated wavelengths. According to our calculations, in a multimode silicon waveguide with a cross-section of $\sim 1600 \times 220 \text{ nm}^2$, conversion between wavelengths separated by 600 THz ($\sim 800 \text{ nm}$) can be achieved (Supplementary Fig. 3).

In conclusion, we have shown that transverse-mode entangled states can be generated and engineered in a multimode silicon waveguide. Combined with previous studies on coherent conversion and manipulation of transverse-mode entanglement [8, 9], the present work shows the potential for realizing complex quantum information processing with high dimensionality and multiple degrees of freedom. Moreover, the multimode waveguide enables much richer nonlinear phenomena than a single-mode waveguide and thus provides an attractive platform for the investigation of nonlinear processes, such as wavelength conversion,

optical soliton fission and super-continuum generation.

MATERIALS AND METHODS

System efficiency. We ascertained the efficiencies for all components using laser light measurements (Supplementary Fig. 4). The one-dimensional grating coupler and 2D grating coupler show coupling losses of 5 dB and 8 dB, respectively. The chip excess losses in our device are 5 dB for the TE_0 mode and 6 dB for the TE_1 mode. The mode multiplexer and demultiplexer induces an excess loss of 0.5 dB on the TE_1 mode. The post-filters and WDMs show an excess loss of 6 dB. The system used for state tomography shows a loss of 2.12 dB and both detectors have an efficiency of 85% (−0.7 dB).

Optical apparatus. We used a CW tunable laser (linewidth 10 kHz, central wavelength 1550.11 nm) as the pump light. The laser was amplified by an erbium-doped fibre amplifier and filtered (100 dB extinction ratio). The remaining power, which was coupled to the device after a single-mode fibre and an on-chip grating coupler, was 6.96 mW, which was then divided into two parts by an on-chip directional coupler to excite the two transverse modes. Fibre alignment was maintained using a piezo-controlled four-dimensional displacement table for the adjustment of the position as well as the coupling angle. The coupling angle was set as 15° and 4° for the one-dimensional grating coupler and 2D grating coupler, respectively. Two off-chip post-filters (100 dB extinction ratio) were used to remove the pump photons, and two WDMs (with an extinction ratio of 30 dB for adjacent channels and 50 dB for non-adjacent channels) were used to separate the signal and idler photons. The correlated photons were recorded by two superconducting nanowire single-photon detectors. The electrical signals were collected and analysed through a time-correlated single photon counting (TCSPC) system, with the coincidence window set as 0.8 ns.

Device fabrication. Chips were fabricated on the most commonly used 220 nm SOI platform. The pattern of the waveguides was exposed on ma-N 2403 negative tone photoresist using electron-beam lithography. The pattern was then transferred to the top silicon layer by an inductively coupled-plasma etching process. Grating couplers were fabricated using a second etching process to achieve efficient fibre-chip coupling. Finally, 1.2 μm plasma enhanced chemical vapour deposition (PECVD) SiO₂ was deposited on the top of the waveguide to form the upper-cladding.

REFERENCES

-
- [1] Horodecki, R., Horodecki, M. & Horodecki, K. Quantum entanglement. *Rev. Mod. Phys.* **81**, 865C942 (2009).
 - [2] Caspani, L. *et al.* Integrated sources of photon quantum states based on nonlinear optics. *Light Sci. Appl.* **6**, e17100 (2017).
 - [3] Matsuda, N. *et al.* A monolithically integrated polarization entangled photon pair source on a silicon chip. *Sci. Rep.* **2**, 817 (2012).
 - [4] Silverstone, J. W. *et al.* On-chip quantum interference between silicon photon-pair sources. *Nature Photon.* **8**, 104-108 (2014).
 - [5] Silverstone, J. W. *et al.* Qubit entanglement between ring-resonator photon-pair sources on a silicon chip. *Nat. Commun.* **6**, 7948 (2015).
 - [6] Kues, M. *et al.* On-chip generation of high-dimensional entangled quantum states and their coherent control. *Nature* **546**, 622-626 (2017).
 - [7] Reimer, C. *et al.* Generation of multiphoton entangled quantum states by means of integrated frequency combs. *Science* **351**, 1176-1180 (2016).
 - [8] Feng, L. T. *et al.* On-chip coherent conversion of photonic quantum entanglement between different degrees of freedom. *Nat. Commun.* **7**, 11985 (2016).
 - [9] Mohanty, A. *et al.* Quantum interference between transverse spatial waveguide modes. *Nat. Commun.* **8**, 14010 (2017).
 - [10] Wang, J., He, S. & Dai, D. On-chip silicon 8-channel hybrid (de) multiplexer enabling simultaneous mode-and polarization-division-multiplexing. *Laser Photonics Rev.* **8**, L18-L22 (2014).
 - [11] Luo, L. W. *et al.* WDM-compatible mode-division multiplexing on a silicon chip. *Nat. Commun.* **5**, 3069 (2014).
 - [12] Stern, B. *et al.* On-chip mode-division multiplexing switch. *Optica* **2**, 530-535 (2015).
 - [13] Gabrielli, L. H., Liu, D., Johnson, S. G. & Lipson, M. On-chip transformation optics for multimode waveguide bends. *Nat. Commun.* **3**, 1217 (2012).
 - [14] Ciampini, M. A. *et al.* Path-polarization hyperentangled and cluster states of photons on a chip. *Light Sci. Appl.* **5**, e16064 (2016).
 - [15] Lanyon, B. P. *et al.* Simplifying quantum logic using higher-dimensional Hilbert spaces. *Nat. Phys.* **5**, 134C140 (2009).
 - [16] Gisin, N., Ribordy, G., Tittel, W. & Zbinden, H. Quantum cryptography. *Rev. Mod. Phys.* **74**, 145C195 (2002).
 - [17] Horodecki, R., Horodecki, P., Horodecki, M. & Horodecki, K. Quantum entanglement. *Rev. Mod. Phys.* **81**, 865-942 (2009).
 - [18] Taillaert, D. *et al.* A compact two-dimensional grating coupler used as a polarization splitter. *IEEE Photon. Tech. Lett.* **15**, 1249-1251 (2003).
 - [19] Wang, J. *et al.* Chip-to-chip quantum photonic interconnect by path-polarization interconversion. *Optica* **3**, 407-413 (2016).
 - [20] James, D. F. V., Kwiat, P. G., Munro, W. J. & White, A. G. Measurement of qubits. *Phys. Rev. A* **64**, 052312 (2001).
 - [21] Harris, N. C. *et al.* Large-scale quantum photonic circuits in silicon. *Nanophotonics* **5**, 456-468 (2016).

- [22] Spring, J. B. *et al.* Boson sampling on a photonic chip. *Science* **339**, 798-801 (2013).
- [23] Metcalf, B. J. *et al.* Quantum teleportation on a photonic chip. *Nature Photon.* **8**, 770-774 (2014).
- [24] Carolan, J. *et al.* Universal linear optics. *Science* **349**, 711-716 (2015).
- [25] Harris, N. C. *et al.* Integrated source of spectrally filtered correlated photons for large-scale quantum photonic systems. *Phys. Rev. X* **4**, 041047 (2014).
- [26] Harris, N. C. *et al.* Quantum transport simulations in a programmable nanophotonic processor. *Nature Photon.* **11**, 447-452 (2017).
- [27] Santagati, R. *et al.* Silicon photonic processor of two-qubit entangling quantum logic. *J. Opt.* **19**, 114006 (2017).
- [28] Wang, J. *et al.* Experimental quantum Hamiltonian learning. *Nat. Phys.* **13**, 551C555 (2017).
- [29] Paesani, S. *et al.* Experimental Bayesian Quantum Phase Estimation on a Silicon Photonic Chip. *Phys. Rev. Lett.* **118**, 100503 (2017).
- [30] Wright, L. G., Christodoulides, D. N. & Wise, F. W. Controllable spatiotemporal nonlinear effects in multimode fibres. *Nature Photon.* **9**, 306-310 (2015).
- [31] Wright, L. G. *et al.* Self-organized instability in graded-index multimode fibres. *Nature Photon.* **10**, 771-776 (2016).
- [32] Pourbeyram, H., Nazemosadat, E. & Mafi A. Detailed investigation of intermodal four-wave mixing in SMF-28: blue-red generation from green. *Opt. Express* **23**, 14487-14500 (2015).
- [33] Ding, Y., Xu, J., Ou, H. & Peucheret, C. Mode-selective wavelength conversion based on four-wave mixing in a multimode silicon waveguide. *Opt. Express* **22**, 127-135 (2014).
- [34] Qiu, Y. *et al.* Mode-selective wavelength conversion of OFDM-QPSK signals in a multimode silicon waveguide. *Opt. Express* **25**, 4493-4499 (2017).
- [35] Garay-Palmett, K. *et al.* Photon-pair generation by intermodal spontaneous four-wave mixing in birefringent, weakly guiding optical fibers. *Phys. Rev. A* **93**, 033810 (2016).
- [36] Karpinski, M., Radzewicz, C. & Banaszek, K. Dispersion-based control of modal characteristics for parametric down-conversion in a multimode waveguide. *Opt. Lett.* **37**, 878-880 (2012).

Acknowledgements

This work was supported by the National Natural Science Foundation of China (NSFC) (Nos. 61590932, 11774333, 61725503, 61431166001), the Anhui Initiative in Quantum Information Technologies (No. AHY130300), the Strategic Priority Research Program of the Chinese Academy of Sciences (No. XDB24030600), the National Key R & D Program (No. 2016YFA0301700), the Zhejiang Provincial Natural Science Foundation of China (Z18F050002), and the Fundamental Research Funds for the Central Universities. This work was partially carried out at the USTC Center for Micro and Nanoscale Research and Fabrication.

Author contributions

All authors contributed extensively to the work presented in this paper. M.Z. and D.X.D. prepared the samples. L.T.F., M.Z., D.X.D and X.F.R. performed the measurements, data analyses and discussions. X.X., Y.C., H.W., M.L., G.P.G. and G.C.G. conducted theoretical analysis. X.F.R. and D.X.D wrote the manuscript and supervised the project.

Additional information

Supplementary information is available in the online version of the paper. Correspondence and requests for materials should be addressed to X.F.R. or D.X.D.

Competing financial interests

The authors declare no competing financial interests.